Haven, CT, 1992); R. A. Engh and R. Huber, *Acta Crystallogr. Sect. A*, 392 (1991).
24. The native I data set was used during the initial model building and in the first stages of refinement, and the native II data set was used for final refinement. The mean figure of merit was 0.66 (25.0 to 3.0 Å). The current model has been refined to a crystallographic *R* factor of 18.4% with the use of data from 8.0 to 2.0 Å resolution with $I/\sigma I > 2.5$ (34,670 unique reflections) and comprises 4115 nonhydrogen protein atoms maintaining strict geometry with deviations from ideal values of bond lengths and angles of 0.010 Å and 1.7°, respectively. It comprises residues 113 to 400, 407 to 507, and 513 to 666 as well as 218 ordered solvent molecules. Residues 109 to 112, 401 to 406, and 508 to 512 and the amino-terminal Met are not defined by electron density and are probably mobile or disordered. The average *B* factors for main chain atoms, side chain atoms, and solvent molecules are 6.7, 9.0, and 19.1 Å^2, respectively. The abbreviations represent the following treatments: HGCR—1 mM mercurochrome (30 hours), 1 M Na_2SO_4, 0.1 M tris-H_2SO_4, (pH 8.0); HGME—0.1 mM MeHgCl (48 hours), 1 M Na_2SO_4, 0.1 M tris-H_2SO_4 (pH 8.0); CMNP—1 mM 2-chloromercuri-4-nitrophenol (1.5 hours), 1 M Na_2SO_4, 0.1 M K_2HPO_4-NaOH (pH 10.0); UOSO—10 mM UO_2SO_4 (2 hours), 1 M Na_2SO_4, 0.1 M NaAc-HAc (pH 5.0); PTL4—2 mM K_2PtCl_4 (6 hours), 1 M Na_2SO_4, 0.1 M K_2HPO_4-NaOH (pH 10.0); CMPT—2 mM K_2PtCl_4, 1 mM 2-chloromercuri-4-nitrophenol (3 hours), 1 M Na_2SO_4, 0.1 M K_2HPO_4-NaOH (pH 10.0).
25. We thank R. Engh, M. Beissinger, and I. Korndoerfer for helpful discussions. Supported by the Deutsche Forschungsgemeinschaft.

11 March 1994; accepted 26 May 1994

High-Resolution Structure of the Oligomerization Domain of p53 by Multidimensional NMR

G. Marius Clore,* James G. Omichinski, Kazuyasu Sakaguchi, Nicola Zambrano, Hiroshi Sakamoto, Ettore Appella, Angela M. Gronenborn*

The three-dimensional structure of the oligomerization domain (residues 319 to 360) of the tumor suppressor p53 has been solved by multidimensional heteronuclear magnetic resonance (NMR) spectroscopy. The domain forms a 20-kilodalton symmetric tetramer with a topology made up from a dimer of dimers. The two primary dimers each comprise two antiparallel helices linked by an antiparallel β sheet. One β strand and one helix are contributed from each monomer. The interface between the two dimers forming the tetramer is mediated solely by helix-helix contacts. The overall result is a symmetric, four-helix bundle with adjacent helices oriented antiparallel to each other and with the two antiparallel β sheets located on opposing faces of the molecule. The tetramer is stabilized not only by hydrophobic interactions within the protein core but also by a number of electrostatic interactions. The implications of the structure of the tetramer for the biological function of p53 are discussed.

The p53 protein is a sequence-specific transcriptional activator that has a key function in tumor suppression (*1*). Inactivation of its tumor suppressor activity, either through mutation or by association with viral or cellular proteins, contributes to the development of as many as 50% of human cancers (*1, 2*). The p53 protein is believed to exert its tumor suppressor activity by stimulating the transcription of the p21 gene product that in turn inhibits cyclin-dependent kinase–4, thereby blocking cell division (*3*). The p53 protein is composed of four domains: an NH_2-terminal transactivation domain, a central DNA binding domain, an oligomerization domain, and a basic COOH-terminal nuclear localization domain (*4*). Although most mutations found in human cancers are located within the DNA binding domain (*2*), several observations suggest that the oligomerization domain may play a key role in cell transformation (*5*). (i) Although wild-type p53 is a tetramer, monomeric p53 (obtained by deletion or mutation of the oligomerization domain) is still capable of tumor suppression. (ii) Many mutants of p53 exert their effects through a negative-dominant mechanism whereby heterotetramers of wild-type and mutant p53 no longer bind DNA sequence specifically or bind with much reduced affinity. (iii) The transforming activity of mutants within the DNA binding domain of p53 can be abolished by making them incapable of forming oligomers as long as wild-type p53 is available from a non-mutant allele. These data suggest that inhibition of p53 oligomerization may be a useful therapeutic avenue for cancer chemotherapy. It has recently been established that a 42–amino acid peptide comprising residues 319 to 360 of p53 constitutes the minimal unit required for tetramerization (*6*). Here, we present the three-dimensional (3D) solution structure of the tetramerization domain (residues 319 to 360) of p53 by means of multidimensional heteronuclear NMR spectroscopy.

Because of the complexity of the system and the necessity to distinguish intra- from intersubunit nuclear Overhauser effects (NOEs), the structure determination was carried out on samples of uniformly labeled

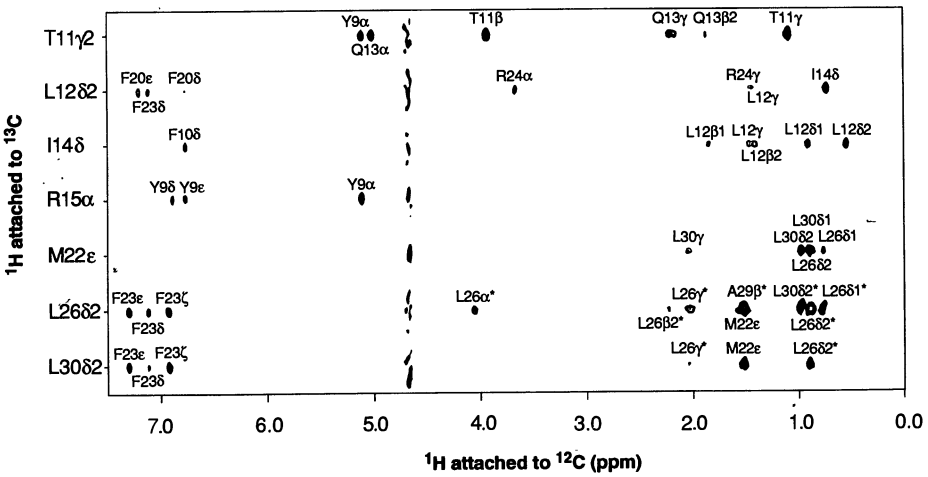

Fig. 1. Composite of ^{13}C–H strips taken from the 3D ^{13}C(*F2*)-edited–^{12}C(*F3*)-filtered NOE spectrum (120 ms mixing time) of the tetrameric oligomerization domain of p53, comprising a 1:1 mixture of unlabeled and ^{13}C-^{15}N–labeled polypeptide and illustrating NOEs between protons of the unlabeled polypeptide (attached to ^{12}C along the *F3* axis) and protons of the labeled peptide (attached to ^{13}C). The NOEs shown with asterisks involve interactions between subunits A and B (and the symmetrically equivalent subunits C and D), whereas the remainder involve interactions between subunits A and C (and the symmetrically equivalent subunits B and D) (*20*).

G. M. Clore, J. G. Omichinski, A. M. Gronenborn, Laboratory of Chemical Physics, Building 5, National Institute of Diabetes and Digestive and Kidney Diseases, National Institutes of Health, Bethesda, MD 20892, USA.
K. Sakaguchi, N. Zambrano, H. Sakamoto, E. Appella, Laboratory of Cell Biology, Building 37, National Cancer Institute, National Institutes of Health, Bethesda, MD 20892, USA.
*To whom correspondence should be addressed.

(^{15}N-^{13}C) protein and on samples of mixed heterotetramers comprising equal amounts of unlabeled and isotopically labeled protein (*7*) and involved the application of double and triple resonance NMR spectroscopy (*8*). The tetramer is completely symmetric, as shown by observation of only a single set of resonances for each residue. Structural information in the form of interproton distance restraints was derived from isotope-edited and isotope-filtered 3D and 4D NOE spectra (*8*). An example of the quality of the data is provided by the composite of $^{13}C(F2) - {}^{1}H(F1)$ strips taken from the 3D ^{13}C-edited $(F2)$–^{12}C-filtered (*F3*) NOE spectrum (Fig. 1), which illustrates specifically intersubunit NOE interactions. The structural statistics for the final ensemble of 30 simulated annealing structures (*9*), calculated on the basis of 3824 experimental NMR restraints, are summarized in Table 1, and a stereo view of a best fit superposition of the backbone atoms is shown in Fig. 2. The first few residues at the NH_2-terminus (residues 319 to 323) and the last COOH-terminal ones (residues 357 to 360) are disordered in solution, as shown by the existence of only intraresidue and sequential NOEs for these residues. The remainder of the tetramer (comprising residues 324 to 356 of each subunit) is very well defined with a precision of 0.38 ± 0.09 Å for the backbone atoms, 0.84 ± 0.06 Å for all atoms, and 0.41 ± 0.08 Å for all atoms that do not exhibit conformational disorder (*10*).

Four views of a schematic ribbon drawing of the tetrameric p53 oligomerization domain are shown in Fig. 3. Each subunit comprises a turn from residues 324 to 325, a strand from residues 326 to 334, a turn from residues 335 to 336, and finally an α helix from residues 337 to 355. The helices form a symmetrical four-helix bundle, with the adjacent helices oriented antiparallel to each other and the non-adjacent opposing helices aligned in a parallel manner. The strands are arranged in two antiparallel β sheets that lie on the outside of the helices and are located on opposite faces of the molecule (Fig. 3, A and C). One sheet is formed by the strands from subunits A (red) and C (yellow), whereas the other is formed by the strands from subunits B (green) and D (blue). Thus, all interactions between subunits A (red) and B (green), subunits A (red) and C (yellow), and subunits A (red) and D (blue) have their symmetrical counterparts in the interactions between subunits C (yellow) and D (blue), subunits B (green) and D (blue), and subunits B (green) and C (yellow), respectively. The tetramer is best described as a dimer of dimers, with AC (red-yellow) and BD (green-blue) forming the primary dimers held together principally by the β sheet structure in addition to helix-helix interactions. The AC (red-yellow) and BD (green-blue) dimers in turn form the subsequent interface solely by means of helix-helix interactions (Fig. 3, C and D). The anatomy of the tetramer as described in this manner is depicted in Fig. 3C. Dimer BD (green-blue) sits on top of dimer AC (red-yellow) at a relative angle of about 130° (the angle between the strands of subunits A and B) (Fig. 3B). To our knowledge, the topology observed here for the p53 oligomerization domain has not been observed previously in other multimeric proteins.

The angles and interhelical separations between the long axes of the two nonequivalent antiparallel helical pairs α_A-α_B and α_A-α_C are 116° and 6.8 Å, and 145° and 8.6 Å, respectively. The corresponding values between the parallel pair α_A-α_D are −76° and 11.7 Å. In terms of the ridges into grooves model of helix packing (*11*), the helix-helix contacts between the antiparallel pairs of helices correspond to class 4-4 packing in which ridges on the helix surface are formed by side chains separated by four residues in the sequence. The angles and separations between the long axes of each strand and the two helices with which it is in contact are 149° and 7.1 Å for the intrasubunit interaction and 19° and 7.3 Å for the intersubunit interaction (that is, the strand from subunit A and the helix from subunit C and the three other symmetrical strand-helix contacts). The β sheet has a characteristic right-handed twist (*11*) with an angle of 163° between the long axes of each strand.

Most hydrophobic contacts are formed between subunits A (red) and C (yellow) [and the symmetrically equivalent subunits B (green) and D (blue)] (Fig. 4A). The hydrophobic core comprising the β strands and helices from subunits A (red) and C (yellow) is formed by van der Waals contacts between Phe^{328} (A), Ile^{332} (C),

Table 1. Structural statistics. The notation of the NMR structures is as follows: ⟨SA⟩ are the final 30 simulated annealing structures; $\overline{SA}$ is the mean structure obtained by averaging the coordinates of the individual SA structures best fitted to each other (excluding residues 319 to 323 and 357 to 360 of all four subunits); and $(\overline{SA})$r is the restrained minimized mean structure obtained by restrained regularization of the mean structure $\overline{SA}$. The number of terms for the various restraints is given in parentheses and applies to the entire tetramer.

Structural statistics	⟨SA⟩	$(\overline{SA})$r
Rms deviations from experimental distance restraints (Å)*		
All (3412)	0.038 ± 0.002	0.018
Intrasubunit		
Interresidue sequential ($\|i - j\| = 1$) (840)	0.032 ± 0.006	0.024
Interresidue short range ($1 < \|i - j\| \leq 5$) (744)	0.042 ± 0.005	0.011
Interresidue long range ($\|i - j\| > 5$) (84)	0.024 ± 0.013	0.012
Intraresidue (744)*	0.023 ± 0.006	0.020
H bond (136)†	0.028 ± 0.010	0.013
Intersubunit		
AB-CD dimer (72)	0.031 ± 0.012	0.009
AC-BD dimer (758)	0.044 ± 0.007	0.015
AD-BC dimer (10)	0	0
H bond (24)†	0.083 ± 0.010	0.022
Rms deviations from $^3J_{HN\alpha}$ coupling constants (Hz) (144)*	0.13 ± 0.02	0.29
Rms deviations from experimental dihedral restraints (degrees) (268)*	0.108 ± 0.036	0.214
Deviations from idealized covalent geometry		
Bonds (Å) (2818)	0.004 ± 0.0002	0.004
Angles (degrees) (5100)	0.507 ± 0.018	0.466
Impropers (degrees) (1444)‡	0.286 ± 0.067	0.499
$E_{L\text{-}J}$ (kcal mol^{-1})§	−660 ± 18	−622

*None of the structures exhibits distance violations greater than 0.3 Å, dihedral angle violations greater than 5°, or $^3J_{HN\alpha}$ coupling constant violations greater than 2 Hz. Furthermore, there are no systematic interproton distance violations between 0.1 and 0.3 Å among the ensemble of calculated structures, and there are no $^3J_{HN\alpha}$ coupling constant violations greater than 1 Hz. All the ϕ,Ψ backbone torsion angles lie within the allowed regions of the Ramachandran plot. The $^3J_{HN\alpha}$ coupling constants included directly in the refinement comprised only those that could be measured from the 3D HNHA experiment to an accuracy of 0.5 Hz or better. Thus, couplings associated with resonances that exhibit overlap of their ^{15}N and NH chemical shifts were not included. The minimum ranges used for the ϕ, χ_1, and χ_2 torsion angle restraints were ±10°, ±20°, and ±20°, respectively (*19*). The narrow range for some of the ϕ restraints was made possible by the availability of highly accurate $^3J_{HN\alpha}$ coupling constant data. In all cases, the angular standard deviations of the torsion angles for the ensemble of 30 SA structures were much smaller than the ranges used for the corresponding torsion angle restraints. Only structurally useful intraresidue NOEs are included in the intraresidue interproton distance restraints. Thus, NOEs between protons separated by two bonds or between nonstereospecifically assigned protons separated by three bonds are not incorporated in the restraints. †For each backbone hydrogen bond there are two distance restraints: $r_{NH\text{-}O}$, 1.7 to 2.5 Å and $r_{N\text{-}O}$, 2.3 to 3.5 Å. These hydrogen bonding restraints were included only in the final stages of refinement. The intersubunit hydrogen bonds involve only the AC and BD dimers. ‡The improper torsion restraints serve to maintain planarity and chirality. §$E_{L\text{-}J}$ is the Lennard-Jones van der Waals energy calculated with the CHARMM (*24*) empirical energy function and is not included in the target function for simulated annealing or restrained minimization.

Gly^{334} (C), and Phe^{338} (C); between Leu^{330} (A), Phe^{338} (C), Phe^{341} (A), the aliphatic portion of the side chain of Arg^{342} (C), and Asn^{345} (C); and between Ile^{332} (A), Phe^{338} (A), and Phe^{341} (A). The hydrophobic helix-helix contacts between subunits A and C involve interactions between Met^{340} (A) and Leu^{348} (C), between Phe^{341} (A), Leu^{344} (C), and Leu^{348} (C); between Leu^{344} (A), Met^{340} (C), Phe^{341} (C), and Leu^{344} (C); and between Leu^{348} (A), the aliphatic portion of the side chain of Arg^{337} (C), Met^{340} (C), and Phe^{341} (C).

The hydrophobic contacts between subunits A (red) and B (green) are more limited in number (Fig. 4B). There is a hydrophobic cluster formed by Met^{340} (A), Leu^{344} (A), Ala^{347} (B), and Leu^{348} (B), between Leu^{350} (A) and Leu^{350} (B), and between the aliphatic portion of the side chain of Lys^{351} (A) and Met^{340} (B). The only hydrophobic contacts observed between subunits A and D are between the methyl groups of Met^{340} (A) and Met^{340} (D) and the methyl groups of Leu^{344} (A) and Leu^{344} (D). The NOE observed between the two former residues in the ^{12}C-filtered–^{13}C-edited NOE spectrum, however, is very weak and below the contour level shown in Fig. 1.

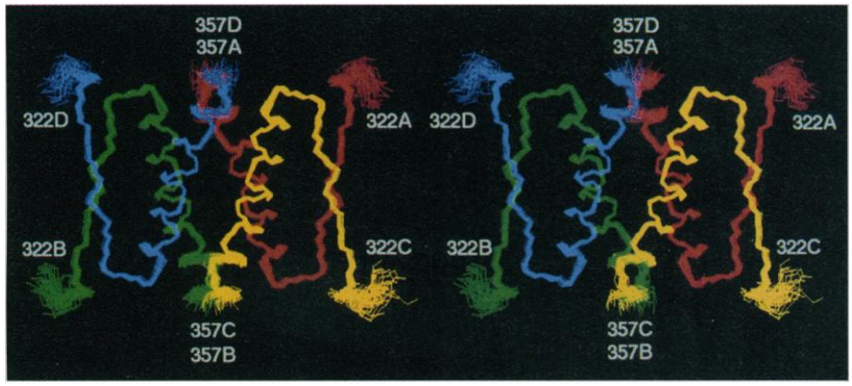

Fig. 2. Stereo view showing a best fit superposition of the backbone (N; Cα, and C) atoms of the 30 simulated annealing (SA) structures of the tetrameric oligomerization domain of p53. The residues shown are 322 to 357, and the color coding of the subunits is as follows: subunit A, red; subunit B, green; subunit C, yellow; and subunit D, blue. The models were generated with the program AVS-XPLOR (*21*).

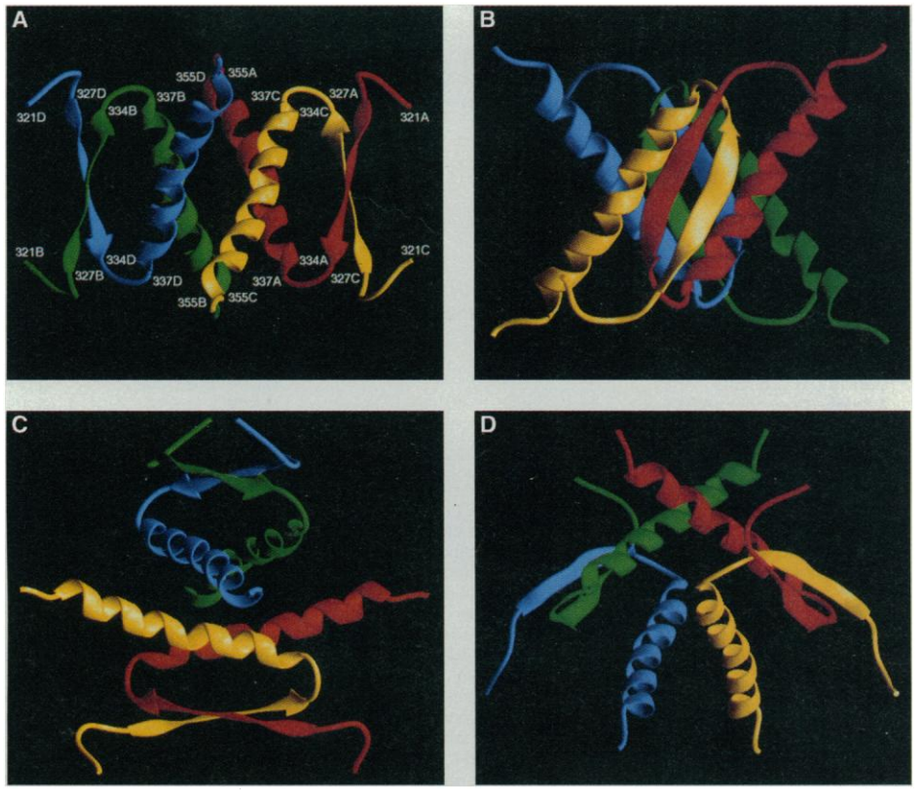

Fig. 3. (**A** through **D**) Four views of a schematic ribbon drawing of the tetrameric oligomerization domain of p53. Subunits A, B, C, and D are shown in red, green, yellow, and blue, respectively. The ribbon diagrams were made with the program RIBBONS (*22*).

The dimerization of subunits A (red) and C (yellow), A (red) and B (green), and A (red) and D (blue) is associated with a decrease in accessible surface area of 1116, 315, and 52 Å^2, respectively, and a solvation free energy of dimerization (*12*) of −10.4, −4.6, and −0.7 kcal mol^{-1}, respectively. Thus, the total decrease in accessible surface area for the tetramer and the total solvation free energy of tetramerization are 6732 Å^2 and −63 kcal mol^{-1}.

In addition to hydrophobic interactions, there are a number of important electrostatic interactions both within each subunit and between the subunits. Within each subunit, the carboxylate of Asp^{324} is hydrogen-bonded to the hydroxyl group of Tyr^{327}, which stabilizes the turn preceding the β strand (Fig. 4A). The interaction between the strand of subunit A (red) and the helix of subunit C (yellow) is stabilized by a salt bridge between the guanidinium group of Arg^{333} (A) and the side chain carbonyl of Asn^{345} (C) and the side chain carboxylate of Glu^{349} (C) (Fig. 4A). The interaction between the helices of subunits A (red) and C (yellow) is stabilized by a salt bridge between the guanidinium groups of Arg^{335} (A) and Arg^{337} (B) and the carboxylate side chain of Asp^{352} (C) (Fig. 4A). Finally, there are two salt bridges involved in stabilizing the interaction between the helices of subunits A (red) and B (green): namely, between the NζH$_3^+$ group of Lys^{351} (A) and the carboxylate side chain of Glu^{339} (B) and between the carboxylate side chain of Glu^{346} (A) and the side chain amide of Gln^{354} (B) (Fig. 4B). The importance of these interactions in maintaining the structure of the tetramer can be ascertained by the fact that (as judged by its ^{1}H NMR spectrum) the structure unfolds below pH 3 (*13*), which is consistent with the protonation of carboxylate side chain groups and the concomitant disruption of the salt bridges.

The structure presented here has a number of important implications with regard to both the function of p53 and protein assembly. In regard to protein assembly, the fold of the tetrameric p53 oligomerization domain clearly demonstrates that the formation of a stable, four-helix bundle does not require the presence of connecting loops. Rather, stabilization can be achieved in other ways, such as here by a pair of antiparallel β sheets located on opposite faces of the tetramer. Indeed, it is likely

that the most crucial element for tetramer formation resides in the two β sheet structures of the AC (red-yellow) and BD (green-blue) dimers. Support for this hypothesis can be drawn from the fact that most stabilizing contacts, as shown by the number of NOEs (Table 1), occur between the β strands and helices of subunits A (red) and C (yellow) (and similarly between subunits B and D). In addition, mutational studies that use fusion proteins of p53 in which the helix has been replaced by a leucine zipper sequence have shown that these proteins fail to form tetramers if either the β strand or part of the strand and connecting loop to the helix have been deleted (*14*), which underscores the importance of this structural element. The structure of the p53 oligomerization domain also highlights the importance of electrostatic interactions, in addition to the hydrophobic interactions within the protein core, for stable tetramer formation. In this regard, the oligomeric p53 tetramerization domain may prove a useful model for studying the folding and assembly of small multimeric systems.

From the point of view of p53 function, the topology of the tetramer places a number of constraints on the relative location of the four DNA binding domains, one from each subunit [residues 102 to 292 (*4*)]. Thus, although the DNA binding domain is connected to the tetramerization domain by a 27-residue linker, it seems likely that the DNA binding domains (residues 102 to 292) of subunits A (red) and C (yellow) are in closer proximity than those of subunits A (red) and B (green) or of subunits A (red) and D (blue) (Fig. 3). [Thus, the Cα–Cα separation between residue 323 of subunits A (red) and C (yellow) is 10 to 12 Å shorter than that between subunits A (red) and B (green) or subunits A (red) and D (blue).] Indeed, the binding sites for p53 typically contain two adjacent, 10-bp palindromes with a Pu-Pu-Pu-C-(A/T)-(A/T)-G-Py-Py-Py consensus sequence (Pu, purine; Py, pyrimidine) (*15*). We therefore suggest that subunits A (red) and C (yellow) contact one palindrome and that subunits B (green) and D (blue) contact the other. Further, the likely disposition of the DNA binding domains of subunits A (red) and C (yellow), relative to those of subunits B (green) and D (blue), suggests that sequence-specific binding of p53 may possibly induce a sizable bend in the DNA. It can be seen from Fig. 3 that the NH_2- and COOH-terminal ends of each subunit of the oligomerization domain are located on the same side of the molecule and are in reasonably close proximity (~20 Å). It is therefore easy to envisage a mechanism whereby the COOH-terminal basic tail of p53 (residues 361 to 393) can modulate the activity of the DNA binding domain (*14*, *16*). It has been observed that recombinant wild-type p53 expressed in *Escherichia coli* displays only weak specific binding in the presence of an intact and unmodified COOH-terminal basic tail and that phosphorylation of Ser^{392}, binding of the monoclonal antibody PAb 421 (whose epitope is located in the COOH-terminal tail), or deletion of the basic COOH-terminal tail results in the activation of strong, sequence-specific binding (*16*). The COOH-terminal basic tail may therefore interfere with specific complex formation either by means of its nonspecific DNA binding properties (*4*) or, perhaps more likely, by interaction with the DNA binding domain, thereby either preventing the latter from adopting the optimal conformation for sequence-specific DNA recognition or masking the DNA recognition site. Removal of the tail by proteolysis, mutagenesis, or binding to an antibody, or modification of the tail by phosphorylation would relieve its inhibitory effects. In this regard, the scissor-type arrangement of the β sheets (Fig. 3) could facilitate rearrangements of the DNA binding domains within the AC (red-yellow) and BD (green-blue) dimers by only minor changes in the interstrand angle, yielding an extremely adaptable and versatile DNA reading mechanism.

Finally, although most of the p53 mutations detected in tumors are located in the DNA binding domain, a few have been observed in the oligomerization domain (*1*, *2*). In addition to a few stop and frameshift mutations, four point mutations have been observed, namely Leu^{330} → His, Gly^{334} → Val, Arg^{335} → Cys, and Glu^{349} → Asp (*17*). Although it has not been shown that these p53 mutants have lost their tumor suppressor activity, they are located at sites involved in the AC (red-yellow) and BD (green-blue) interfaces (Fig. 4A) and could therefore potentially destabilize the tetramer, thereby disrupting or partially disrupting oligomerization. Specifically, the Leu^{330} → His mutation would introduce a hydrophilic residue within the center of the

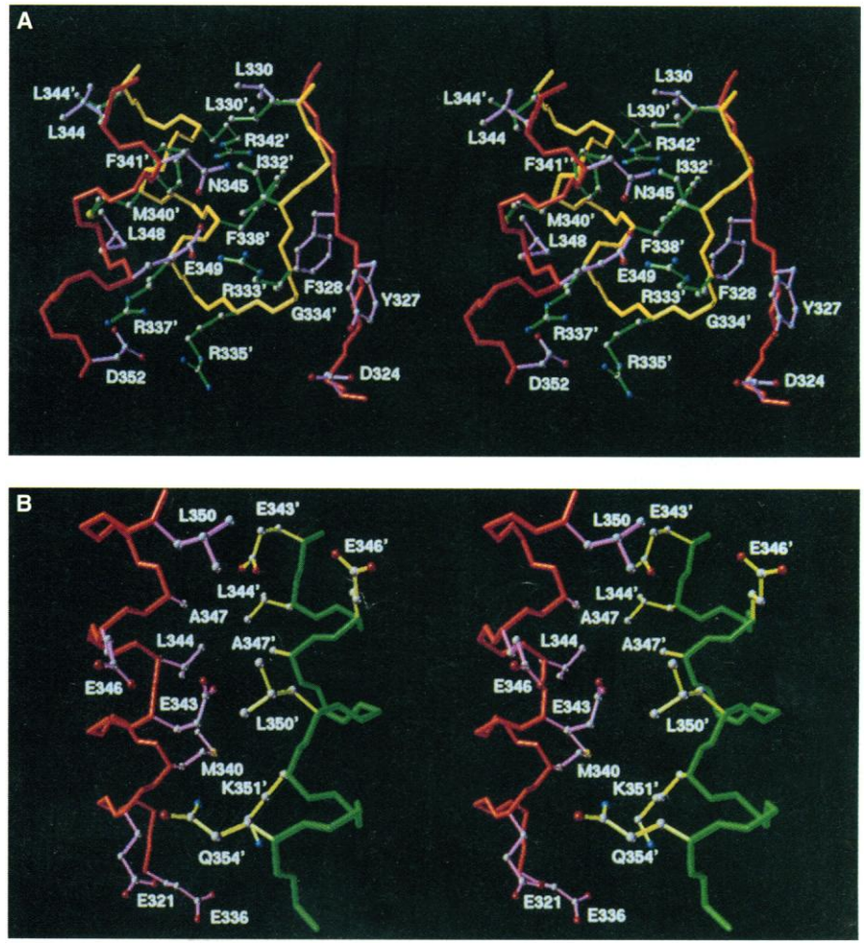

Fig. 4. Stereo views illustrating the interface between (**A**) the A and C subunits and (**B**) the A and B subunits. The backbone atoms of the A, B, and C subunits are shown in red, green, and yellow, respectively; the side chains of the A, B, and C subunits are shown in purple, yellow, and green, respectively. The models were generated with the program VISP (*23*).

hydrophobic core comprising the β sheet and the helices from subunits A and C; the Gly^{334} → Val mutation (subunit A) would introduce steric clash with the side chain of Phe^{328}, the Cα of Tyr^{327}, and the backbone carbonyl of Glu^{326} and therefore is likely to disrupt the end of the β sheet and to destabilize the turn (residues 335 to 336) linking the β strand and the helix; the Arg^{335} → Cys mutation would remove the electrostatic interaction between Arg^{335} of subunit A and Glu^{349} of subunit C; likewise, the replacement of Glu^{349} by the shorter Asp side chain would either remove or reduce the strength of the electrostatic interaction between Arg^{335} of subunit A and Glu^{349} of subunit C.

REFERENCES AND NOTES

1. A. J. Levine, J. Momand, C. A. Finlay, *Nature* **351**, 453 (1991); B. Vogelstein and K. W. Winzler, *Cell* **70**, 523 (1992); D. P. Lane, *Nature* **358**, 15 (1992); L. A. Donehower and A. Bradley, *Biochim. Biophys. Acta* **1155**, 181 (1993).
2. M. Hollstein, D. Sidransky, B. Volgelstein, C. C. Harris, *Science* **253**, 49 (1991); C. C. Harris, *ibid.* **262**, 1980 (1993).
3. Y. Xiong *et al.*, *Nature* **366**, 701 (1993); W. S. El-Deiry *et al.*, *Cell* **75**, 817 (1993); V. Dulic *et al.*, *ibid.* **76**, 1013 (1994).
4. N. T. Unger, N. M. Mau, S. Segal, J. Minna, *EMBO J.* **11**, 1383 (1992); C. Prives and J. J. Manfredi, *Genes Dev.* **7**, 529 (1993); N. P. Pavletich, K. A. Chambers, C. O. Pabo, *ibid.*, p. 2556; J. Bargonetti *et al.*, *ibid.*, p. 2565; Y. Wang *et al.*, *ibid.*, p. 2575.
5. J. M. Slingerland, J. R. Jenkins, S. Benchimol, *EMBO J.* **12**, 1029 (1993); E. Shaulian *et al.*, *ibid.*, p. 2789; P. N. Friedman, X. Chen, J. Bargonetti, C. Prives, *Proc. Natl. Acad. Sci. U.S.A.* **90**, 3319 (1993).
6. H. Sakamoto *et al.*, *Proc. Natl. Acad. Sci. U.S.A.*, in press.
7. The DNA coding sequence for residues 319 to 360 of p53 (*1*) was generated as a Nde I–Bam HI DNA fragment with the polymerase chain reaction [S. J. Scharf, G. T. Horn, H. A. Erlich, *Science* **233**, 1076 (1986)], cloned into the *E. coli* vector pET12A, and expressed in the host bacterial strain BL21(DE3) [F. W. Studier, A. H. Rosenberg, J. J. Dunn, J. W. Dubendorf, *Methods Enzymol.* **185**, 60 (1990)]. The p53 oligomerization peptide was uniformly (>95%) labeled with either ^{15}N or with ^{15}N and ^{13}C by growing the bacteria in minimal medium with $^{15}NH_4Cl$ or both $^{15}NH_4Cl$ and $^{13}C_6$-glucose as the sole nitrogen and carbon sources, respectively. Cells were grown overnight at 37°C, diluted with salts (1:4), and then induced for 4 hours at 37°C with 0.5 mM isopropyl-β-D-thiogalactoside. The cells were harvested, resuspended in 100 mM tris buffer (pH 7.2), 5 mM EDTA, 5 mM benzamidine, and 1 mM dithiothreitol (DTT), lysed by passage through a French press, and centrifuged at 20,000*g* for 30 min. The supernatant was removed, centrifuged at 100,000*g* for 1 hour, and then applied to a DEAE-Sepharose Fast Flow (Pharmacia) column (200-ml bed volume) equilibrated with buffer A [100 mM tris (pH 7.2), 5 mM EDTA, and 1 mM DTT]. Fractions containing the p53 peptide were pooled and diluted to give a final buffer concentration of 25 mM tris (pH 7.2), 5 mM EDTA, and 1 mM DTT (buffer B). The sample was then applied to a Q-Sepharose Fast Flow (Pharmacia) column (200-ml bed volume) equilibrated with buffer B. The p53 peptide was eluted with a 0 to 1 M NaCl gradient in buffer B, and the fractions containing the desired product were pooled. The latter was further purified on a C-4 reversed-phase (Vydac) high-performance liquid chromatography column with a 15 to 40% acetonitrile gradient over 25 min in 0.05% aqueous trifluoroacetic acid. The purified peptide was taken up in water and the final pH adjusted to 6.8. Five samples were used for NMR spectroscopy: uniformly ^{15}N-labeled p53 peptide (2.8 mM) in 90% H_2O–10% D_2O; uniformly ^{15}N-^{13}C–labeled p53 peptide (2.8 mM) in 90% H_2O–10% D_2O and in 99.996% D_2O; and a 1:1 mixture of unlabeled (2.5 mM) and ^{15}N-^{13}C uniformly labeled (2.5 mM) p53 peptide in 90% H_2O–10% D_2O and in 99.996% D_2O. In the case of the latter samples, the following procedure was used to ensure random association of the monomers into the tetrameric form: The dry peptides were first dissolved in 0.05% aqueous trifluoroacetic acid and then dissociated with acetonitrile at a final ratio of 75% acetonitrile/25% H_2O and a final peptide concentration of 0.05 mM. This solution was then taken to dryness, reconstituted in water to give a final peptide concentration of 5 mM (2.5 mM labeled and 2.5 mM unlabeled), and the tetramer reassociated by raising the pH to 6.8 with NaOH. The association constant for the monomer-tetramer equilibrium is 2.5×10^{17} M^{-3} (*6*), so that under the experimental conditions used, the concentration of tetramer present was greater than 99%.
8. All NMR experiments were carried out at 35°C on a Bruker AMX600 spectrometer equipped with a *z*-shielded gradient triple resonance probe. The sequential assignment of the ^1H, ^{13}C, and ^{15}N chemical shifts of the tetramerization domain of p53 (residues 319 to 360) was achieved by means of through-bond heteronuclear correlations along the backbone and side chains with the following 3D experiments: ^{15}N-separated HOHAHA, HNHA, CBCANH, CBCA(CO)NH, HBHA(CO)NH, C(CO)NH, H(CCO)NH, HCCH-correlated spectroscopy (COSY), and HCCH–total correlation spectroscopy to demonstrate CαH(*i*)/CβH(*i*)-^{15}N(*i*)-NH(*i*), CαH(*i*)-^{15}N(*i*)-NH(*i*), ^{13}Cβ/Cα(*i*)-^{15}N(*i*)-NH(*i*) and ^{13}Cβ/Cα(*i* − 1)-^{15}N(*i*)-NH(*i*), ^{13}Cβ/Cα(*i* − 1)-^{15}N(*i*)-NH(*i*), CβH/CαH(*i* − 1)-^{15}N(*i*)-NH(*i*), $^{13}C_j$(*i* − 1)-^{15}N(*i*)-NH(*i*), H_j(*i* − 1)-^{15}N(*i*)-NH(*i*), H_j-$^{13}C_j$-$^{13}C_{j\pm1}$-$H_{j\pm1}$ and H_j-$^{13}C_j$-$^{13}C_{j\pm n}$-$H_{j\pm n}$ correlations, respectively (*i* refers to the residue number and *j* to the carbon position along a side chain). Details of these experiments and original references are provided [A. Bax and S. Grzesiek, *Acc. Chem. Res.* **26**, 131 (1993); G. M. Clore and A. M. Gronenborn, *Prog. Nucl. Magn. Reson. Spectrosc.* **23**, 43 (1991); G. W. Vuister *et al.*, *Methods Enzymol.* **239**, 79 (1994); G. M. Clore and A. M. Gronenborn, *ibid.*, p. 349]. Quantitative $^3J_{HN\alpha}$, $^3J_{CC}$, $^3J_{C\gamma N}$, $^3J_{C\gamma CO}$, and $^3J_{\alpha\beta}$ couplings were measured from a 3D HNHA spectrum [G. W. Vuister and A. Bax, *J. Am. Chem. Soc.* **115**, 7772 (1993)], a 2D long-range, carbon-carbon correlation spectrum [A. Bax, D. Max, D. Zax, *ibid.* **114**, 6923 (1992)], a 2D ^{13}C-{^{15}N}-spin-echo difference constant time heteronuclear single quantum coherence (HSQC) spectrum [G. Vuister, A. Wang, A. Bax, *J. Magn. Reson.* **115**, 5334 (1993)], a 2D ^{13}C-{^{13}CO}-spin-echo difference constant time HSQC spectrum [S. Grzesiek, G. W. Vuister, A. Bax, *J. Biomol. NMR* **3**, 487 (1993)], and a 2D ^1H-^1H primitive exclusive COSY spectrum [L. Mueller, *J. Magn. Reson.* **72**, 191 (1987)], respectively. Qualitative $^3J_{\alpha\beta}$, $^3J_{NH\beta}$, and $^3J_{COH\beta}$ couplings were obtained from 3D ^{15}N-separated HOHAHA (*18*), HNHB [S. J. Archer *et al.*, *ibid.* **95**, 636 (1991)], and HN(CO)HB [S. Grzesiek, M. Ikura, G. M. Clore, A. M. Gronenborn, A. Bax, *ibid.* **96**, 215 (1992)] experiments, respectively. NOEs between NH protons were assigned from a 3D ^{15}N-separated NOE spectrum [D. Marion *et al.*, *Biochemistry* **28**, 6150 (1989); E. R. P. Zuiderweg and S. W. Fesik, *ibid.*, p. 2387] and 3D ^1H-^{15}N heteronuclear multiple-quantum coherence–NOE–^1H-^{15}N HSQC spectrum [M. Ikura, A. Bax, G. M. Clore, A. M. Gronenborn, *J. Am. Chem. Soc.* **112**, 9020 (1990)] recorded with mixing times of 110 and 120 ms, respectively. NOEs between ^{15}N-attached and ^{13}C-attached protons and between ^{13}C-attached protons only were derived from 4D ^{15}N-^{13}C–separated [L. E. Kay, G. M. Clore, A. Bax, A. M. Gronenborn, *Science* **249**, 411 (1990)] and 4D ^{13}C-^{13}C–separated [G. M. Clore, L. E. Kay, A. Bax, A. M. Gronenborn, *Biochemistry* **30**, 12 (1991); G. W. Vuister *et al.*, *J. Magn. Reson. Ser. B* **101**, 210 (1993)] NOE spectra, respectively, recorded with a mixing time of 110 ms. In the mixed 1:1 labeled and unlabeled samples, NOEs from ^{14}N and ^{12}C-attached protons to ^{15}N-attached protons and from ^{13}C-attached protons to ^{12}C-attached protons were assigned from 3D ^{12}C-^{14}N–filtered (*F1*)–^{15}N(*F2*)-edited and ^{13}C-edited(*F2*)–^{12}C-filtered(*F3*) NOE spectra, respectively, recorded with a mixing time of 120 ms [M. Ikura *et al.*, *Science* **256**, 632 (1992); J. G. Omichinski *et al.*, *ibid.* **261**, 438 (1993)]. The interproton distance restraints were grouped into four ranges: 1.8 to 2.7 Å (1.8 to 2.9 Å for NOEs involving NH protons), 1.8 to 3.3 Å (1.8 to 3.5 Å for NOEs involving NH protons), 1.8 to 5.0 Å, and 1.8 to 6.0 Å, corresponding to strong, medium, weak, and very weak NOEs, respectively [M. P. Williamson, T. F. Havel, K. Wüthrich, *J. Mol. Biol.* **182**, 295 (1985); G. M. Clore *et al.*, *EMBO J.* **5**, 2729 (1986)]. Upper distance limits for distances involving methyl protons and nonstereospecifically assigned methylene protons were corrected appropriately for center averaging [K. Wüthrich, M. Billeter, W. Braun, *J. Mol. Biol.* **169**, 949 (1983)]. In addition, 0.5 Å was added to the upper limit of distances involving methyl protons to account for the higher apparent intensity of methyl resonances [G. M. Clore, A. M. Gronenborn, M. Nilges, C. A. Ryan, *Biochemistry* **26**, 8012 (1987)]. Stereospecific assignments and φ and χ_1 torsion angle restraints were obtained with the conformational grid search program STEREOSEARCH [M. Nilges, G. M. Clore, A. M. Gronenborn, *Biopolymers* **29**, 813 (1990)] on the basis of the $^3J_{HN\alpha}$ and $^3J_{\alpha\beta}$ coupling constants and intraresidue and sequential interresidue interproton distance restraints involving the NH, CαH, and CβH protons derived from 3D ^{15}N- and ^{13}C-separated rotating frame Overhauser enhancement spectroscopy (ROESY) experiments (35 ms and 30 ms mixing times, respectively) [G. M. Clore, A. Bax, P. T. Wingfield, A. M. Gronenborn, *Biochemistry* **29**, 5671 (1990)] (*18*). Information from $^3J_{NH\beta}$ and $^3J_{COH\beta}$ coupling constants was also used for identifying the appropriate χ_1 rotamer and for detecting rotamer averaging. Finally, χ_2 torsion angle restraints for Leu residues were obtained from $^3J_{CC}$ coupling constants and the pattern of intraresidue NOEs [R. Powers *et al.*, *Biochemistry* **32**, 6744 (1993)].
9. The structures were calculated with the hybrid distance, geometry-simulated annealing protocol [M. Nilges, G. M. Clore, A. M. Gronenborn, *FEBS Lett.* **229**, 317 (1988)], which makes use of the program X-PLOR-31 [A. T. Brünger, *X-PLOR Version 3.1: A System for X-ray Crystallography and NMR* (Yale Univ. Press, New Haven, CT, 1993)] with minor modifications to ensure symmetry (*19*). The target function that is minimized during simulated annealing comprises only quadratic harmonic potential terms for covalent geometry (that is, bonds, angles, planes, and chirality), square-well quadratic potentials for the experimental distance and torsion angle restraints, a harmonic potential for the $^3J_{HN\alpha}$ coupling constant restraints [D. S. Garrett *et al.*, *J. Magn. Reson. Ser. B* **104**, 99 (1994); (*19*)], an effective harmonic potential to maintain symmetry between the two subunits, and a quartic van der Waals repulsion term for the nonbonded contacts. No hydrogen bonding, electrostatic, or 6–12 Lennard-Jones empirical potential energy terms were present in the target function. The topology of the tetramer was established as follows. A qualitative interpretation of the NOE data involving the NH and CαH protons, the $^3J_{HN\alpha}$ coupling constants, and the $^{13}C\alpha$ and $^{13}C\beta$ chemical shifts permitted the unambiguous delineation of the secondary structure consisting of a helix (residues 337 to 355) and a β strand (residues 326 to 334) that was paired with the same β strand from another subunit in the form of an antiparallel β sheet. In addition, the observation of NOEs from Arg^{337}, Met^{340}, and Phe^{341} to Leu^{348} and from Glu^{339}, Met^{340}, and Glu^{345} to Lys^{351} indicated unambig-

uously that the helices of the four subunits had to be arranged in an antiparallel manner. Thus, from considerations of symmetry we could readily ascertain that the basic topology consisted of a four-helix bundle and a pair of antiparallel β sheets. Initial calculations were therefore carried out on the basis of the following NOEs: unambiguous intrasubunit NOEs relating to the secondary structure; intersubunits relating to the two antiparallel β sheets, one between subunits A and C, the other between subunits B and D (overlap of the two sheets could be unambiguously excluded from a qualitative interpretation of the NOE data as well as considerations of symmetry), and intersubunit NOEs that could not be partitioned into particular intersubunit interactions and were therefore treated as r_{ij}^{-6} sum averages (where r is distance) to allow the computer to partition any given restraint between all pairwise subunit interactions [M. Nilges, *Proteins Struct. Funct. Genet.* **17**, 297 (1993)]. With this pairing of the β strands, the interactions between the A and B subunits are symmetrically equivalent to those between the C and D subunits, the interactions between the A and C subunits are symmetrically equivalent to the interactions between the B and D subunits, and the interactions between the A and D subunits are symmetrically equivalent to those between the B and C subunits. In addition to the initial structure calculations, a physical model was built on the basis of the data and proved to be very helpful in sorting out the tetramer arrangement. Once the tetramer topology was clearly established from the initial structure calculations, an iterative strategy was used to assign all structurally useful intra- and intersubunit NOEs explicitly. The final structure calculations were based on 3252 approximate interproton distance restraints (2412 intra- and 840 intersubunit, partitioned into 758 for the AC and BD subunits, 72 for the AB and CD subunits, and 10 for the AD and BC subunits). These were supplemented by 160 distance restraints for 68 intra- and 12 intersubunit hydrogen bonds, 268 torsion angle restraints (144 ϕ, 104 χ_1, and 20 χ_2), 144 $^3J_{HN\alpha}$ coupling constant restraints, and stereospecific assignments for 104 of the 144 β methylene groups and for the methyl groups of all 16 Leu residues. (The number of restraints and stereospecific assignments applies to the tetramer; as the tetramer is completely symmetric, each observed NOE, for example, gives rise to four interproton distance restraints, one for each subunit.) The coordinates of the 30 final simulated annealing (SA) structures of the tetrameric oligomerization domain of p53, together with the coordinates of the restrained minimized mean structure, $\langle SA \rangle$r, and the complete list of experimental NMR restraints and ^{1}H, ^{15}N, and ^{13}C assignments have been deposited in the Brookhaven Protein Data Bank.

10. The precision of the atomic coordinates is defined as the average root mean square difference between the individual simulated annealing structures and the mean coordinate positions. The atoms that do not exhibit conformational disorder comprise all N, Cα, C, O, and Cβ atoms of residues 324 to 356 of the four subunits, the complete side chains of Y327, F328, T329, L330, I332, F338, M340, F341, L344, L348, L350, the side chains of D324, E326, E331, R333, R335, R337, E339, E343, E346, E349, and D352 up to Cγ, and the side chains of R24 up to Cδ and K351 up to Cε (*20*).
11. C. Chothia *et al.*, *J. Mol. Biol.* **145**, 215 (1981).
12. D. Eisenberg and A. D. McLachlan, *Nature* **319**, 199 (1986); L. Cliche *et al.*, *Proc. Natl. Acad. Sci. U.S.A.* **87**, 3240 (1990).
13. At pH 2.5, the dispersion of the ^{1}H chemical shifts is typical of a random coil peptide.
14. T. D. Halazonetis and A. N. Kandil, *EMBO J.* **12**, 5057 (1993); J. A. Pietenpol *et al.*, *Proc. Natl. Acad. Sci. U.S.A.* **91**, 1998 (1994).
15. S. E. Kern *et al.*, *Science* **252**, 1708 (1991); W. D. Funk *et al.*, *Mol. Cell. Biol.* **12**, 2866 (1992).
16. T. R. Hupp *et al.*, *Cell* **71**, 875 (1992).
17. F.-S. Liu *et al.*, *Obstet. Gynecol.* **83**, 118 (1994); D. D'Amico *et al.*, *Oncogene* **7**, 339 (1992); N. Nishida *et al.*, *Cancer Res.* **53**, 368 (1993); H. Miyamoto *et al.*, *Oncology Res.* **5**, 245 (1993).
18. G. M. Clore *et al.*, *J. Biomol. NMR* **1**, 13 (1991).
19. G. M. Clore *et al.*, *Biochemistry* **29**, 1689 (1990); P. J. Lodi *et al.*, *Science* **263**, 1762 (1994).
20. Abbreviations for the amino acid residues are: A, Ala; C, Cys; D, Asp; E, Glu; F, Phe; G, Gly; H, His; I, Ile; K, Lys; L, Leu; M, Met; N, Asn; P, Pro; Q, Gln; R, Arg; S, Ser; T, Thr; V, Val; W, Trp; and Y, Tyr.
21. W. DeLano and A. T. Brünger, *AVS-XPLOR User's Manual* (Yale University, New Haven, CT, 1993).
22. M. Carson, *J. Mol. Graphics* **5**, 103 (1987).
23. E. De Castro and S. Edelstein, *VISP 1.0 User's Guide* (University of Geneva, Geneva, 1992).
24. B. R. Brooks *et al.*, *J. Comput. Chem.* **4**, 187 (1983).
25. Supported by the AIDS Directed Anti-Viral Program of the Office of the Director of NIH (G.M.C., A.M.G., and E.A.). We thank J. Huth for generously providing suitably prepared pET12A vector DNA and M. Greenblatt and C. Harris for useful discussions.

10 May 1994; accepted 13 June 1994

Potential Role of Human Cytomegalovirus and p53 Interaction in Coronary Restenosis

Edith Speir,* Rama Modali, Eng-Shang Huang, Martin B. Leon, Fayaz Shawl, Toren Finkel, Stephen E. Epstein

A subset of patients who have undergone coronary angioplasty develop restenosis, a vessel renarrowing characterized by excessive proliferation of smooth muscle cells (SMCs). Of 60 human restenosis lesions examined, 23 (38 percent) were found to have accumulated high amounts of the tumor suppressor protein p53, and this correlated with the presence of human cytomegalovirus (HCMV) in the lesions. SMCs grown from the lesions expressed HCMV protein IE84 and high amounts of p53. HCMV infection of cultured SMCs enhanced p53 accumulation, which correlated temporally with IE84 expression. IE84 also bound to p53 and abolished its ability to transcriptionally activate a reporter gene. Thus, HCMV, and IE84-mediated inhibition of p53 function, may contribute to the development of restenosis.

Coronary angioplasty causes vessel wall injury and induces a SMC proliferative response similar to the healing response of other tissues to injury. This response is so excessive in 25 to 50% of patients that it leads to coronary restenosis. On the basis of a proposal that atherosclerosis (also characterized by SMC proliferation) might be a form of benign neoplasia (*1*), we hypothesized that formation of the neointimal lesion during restenosis may be driven by alterations that confer to cells a selective growth advantage; upon activation, as by injury, such cells would undergo excessive proliferation.

We investigated two molecular mechanisms that might contribute to the abnormal SMC proliferation: (i) aberrant expression of p53, a tumor suppressor protein that inhibits cell cycle progression and that is functionally inactivated in many human cancers (*2*); and (ii) activation of latent HCMV, a herpesvirus that has been associated with the development of atherosclerosis (*3*). Conceivably, an HCMV protein or proteins could impair p53's growth suppressor function, as is the case for proteins encoded by several DNA tumor viruses (*4*, *5*).

We studied 60 patients (age 36 to 89 years; mean 59) who had undergone primary balloon angioplasty for severe symptoms secondary to coronary artery disease. Each had a satisfactory angiographic result at the time of angioplasty but later developed recurrent angina and were subsequently found to have stenosis at the site of angioplasty. Coronary atherectomy was performed 1 to 6 months after angioplasty, and the specimens obtained from such patients are referred to here as restenosis lesions. Atherectomy tissue was also obtained from an additional 20 patients who were undergoing atherectomy for angina but who had not previously undergone angioplasty. These specimens are referred to as primary lesions. The restenosis lesions were firm, cylindrical fragments 1 to 5 mm long and 0.2 to 0.4 mm in diameter. They were cellular and nearly all cells were identifiable as SMCs by immunostaining with an antibody to muscle actin (*6*). In contrast, primary lesions were hypocellular and often contained thrombus.

In normal cells, wild-type p53 has a short half-life (5 to 20 min) (*7*) and hence

E. Speir, T. Finkel, S. E. Epstein, Cardiology Branch, National Institutes of Health, Bethesda, MD 20892, USA.
R. Modali, BioServe Biotechnologies Limited, Laurel, MD 20707, USA.
E.-S. Huang, Lineberger Comprehensive Cancer Center, University of North Carolina, Chapel Hill, NC 27599, USA.
M. B. Leon, Washington Cardiology Center, Division of Cardiology, Washington Hospital Center, Washington, DC 20010–2975, USA.
F. Shawl, Department of Cardiology, Washington Adventist Hospital, Takoma Park, MD 20912, USA.
*To whom correspondence should be addressed.